View Article Online
View Journal

Lab on a Chip

Accepted Manuscript

This article can be cited before page numbers have been issued, to do this please use: P. Doyle, K. W. Bong and J. Lee, *Lab Chip*, 2014, DOI: 10.1039/C4LC00877D.

This is an *Accepted Manuscript*, which has been through the Royal Society of Chemistry peer review process and has been accepted for publication.

Accepted Manuscripts are published online shortly after acceptance, before technical editing, formatting and proof reading. Using this free service, authors can make their results available to the community, in citable form, before we publish the edited article. We will replace this *Accepted Manuscript* with the edited and formatted *Advance Article* as soon as it is available.

You can find more information about *Accepted Manuscripts* in the Information for Authors.

Please note that technical editing may introduce minor changes to the text and/or graphics, which may alter content. The journal's standard Terms & Conditions and the Ethical guidelines still apply. In no event shall the Royal Society of Chemistry be held responsible for any errors or omissions in this *Accepted Manuscript* or any consequences arising from the use of any information it contains.

ROYAL SOCIETY OF CHEMISTRY

www.rsc.org/loc

Stop Flow Lithography in Perfluoropolyether (PFPE) Microfluidic Channels

View Article Online
DOI: 10.1039/C4LC00877D

Ki Wan Bong[a,b] , Jiseok Lee [a,c], and Patrick S. Doyle*[a]

Received (in XXX, XXX) Xth XXXXXXXXX 20XX, Accepted Xth XXXXXXXXX 20XX
DOI: 10.1039/b000000x

Stop Flow Lithography (SFL) is a microfluidic-based particle synthesis method for creating anisotropic multifunctional particles with applications that range from MEMs to biomedical engineering. Polydimethylsiloxane (PDMS) has been typically used to construct SFL devices as the material enables rapid prototyping of channels with complex geometries, optical transparency, and oxygen permeability. However, PDMS is not compatible with most organic solvents which limit the current range of materials that can be synthesized with SFL. Here, we demonstrate that a fluorinated elastomer, called perfluoropolyether (PFPE), can be an alternative oxygen permeable elastomer for SFL microfluidic flow channels. We fabricate PFPE microfluidic devices with soft lithography and synthesize anisotropic multifunctional particles in the devices via the SFL process - this is the first demonstration of SFL with oxygen lubrication layers in a non-PDMS channel. We benchmark the SFL performance of the PFPE devices by comparing them to PDMS devices. We synthesized particles in both PFPE and PDMS devices under the same SFL conditions and found the difference of particle dimensions was less than a micron. PFPE devices can greatly expand the range of precursor materials that can be processed in SFL because the fluorinated devices are chemically resistant to most organic solvents, an inaccessible class of reagents in PDMS-based devices due to swelling.

Introduction

Stop Flow Lithography (SFL) is a synthesis technique for creating microparticles with complex morphologies and chemical patterns[1-6]. In one cycle of SFL, photopatternable monomers are introduced to a microchannel, the flow quickly stopped, a brief pulse of UV light creates particles which are then flushed out of the device. During the photopolymerization step, particle geometries are defined by masks and channel topographies. Also, distinct chemical regions in particles are defined by flow patterns that can be precisely adjusted via microfluidic modulation. The combination of photolithography and microfluidic techniques allows independent control over particle size, shape, and even chemical patchiness. Using this *in situ* fabrication method, diverse multifunctional particles have been prepared for new applications in the fields of diagnostics[7-11], assembly[12-14], MEMS[15], photonics[16], and tissue engineering[17]. In addition to particles, recently polymeric sheets have been fabricated with SFL[18].

The current SFL protocol has several requirements in device construction[1, 2]. (1) The channel material should be compatible with soft lithography to allow rapid prototyping of channels with various geometries. SFL devices have been fabricated with multiple inlet pathways or layered channels to create structured micro-flows for the synthesis of chemically patterned particles[1-8]. (2) Flow channels must be optically transparent as particles are synthesized by shining a burst of UV light through the device. (3) Oxygen permeable flow channels are necessary because the process requires local inhibition of polymerization near channel interfaces via oxygen permeation. By virtue of this localized inhibition layer, particles can be advected through flow without sticking to the device walls.

To date, polydimethylsiloxane (PDMS) devices have been predominately used in SFL process as they satisfy all the aforementioned criteria. Using soft-lithography, PDMS afford easy and rapid fabrication of microfluidic devices[19, 20]. Complex layouts of microfluidic channels have been created by simply casting PDMS prepolymer onto a silicon master containing positive relief features[19]. PDMS is optically transparent, compatible with standard photolithography techniques, and has low-autofluorescence[21]. By having a large gas permeability[22], PDMS devices allow sufficient diffusion of oxygen to inhibit radical polymerization near the surface[23]. Because of these advantages, PDMS devices have been predominantly used for SFL. PDMS devices for SFL applications, however, have considerable limitations, namely undesirable swelling in most organic solvent flows[24], limiting the range of precursor materials which can be processed.

Previous researchers have noticed the poor solvent resistance of PDMS devices for their applications, replacing PDMS with other polymeric materials such as thiolene-based resins[25-28], polycarbonate[29, 30], polyethylene glycol[31], polyimide[32, 33], polyurethane acrylate (PUA)[34, 35], polymethylmethacrylate[36], Teflon[37], and poly(silazane)[38]. In lieu of substitution of the material of the device, various methods to modify the surface of PDMS devices have been also proposed to overcome the limitations and expand the versatility of PDMS-based microfluidics[39, 40]. In their attempts to replace or improve PDMS,

[a] *Department of Chemical Engineering, Massachusetts Institute of Technology, 77 Massachusetts Avenue, Cambridge, MA 02139, USA E-mail: pdoyle@mit.edu, Fax: +1 617 258 5042; Tel: +1 617 253 4534*
[b] *Department of Chemical and Biological Engineering, Korea University, Anam-dong, Sungbuk-ku, Seoul 136-713, Korea*
[c] *School of Energy and Chemical Engineering, Ulsan National Institute of Science and Technology, Eonyang-eup, Ulju-gun, Ulsan 689-798, Korea*

Published on 07 October 2014. Downloaded on 07/10/2014 16:17:00.

Lab on a Chip Accepted Manuscript

View Article Online
DOI: 10.1039/C4LC00877D

microfluidic devices with solvent resistance have been successfully developed, yet most of these devices are significantly less permeable to oxygen, preventing their application in SFL.

Liquid perfluoropolyether (PFPE) has been recently suggested as an alternative material for the fabrication of solvent resistant microfluidic devices[41-44]. Homogeneous PFPE devices have exhibited chemical resistances against most organic solvents, acids, and alkali[41-44]. Furthermore, Unger *et al.* demonstrated that multi-layered PFPE devices can be created from commercially available and heat-curable PFPEs. The authors used a simple soft lithography similar to the PDMS process of mixing, casting, and curing during device construction[44]. Most importantly, the fluorinated PFPE elastomer has shown optical transparency and large oxygen permeability[42]

Utilizing these advantages of PFPE, we here demonstrate SFL in PFPE microfluidic channels. We show that PFPE can provide oxygen lubrication layers for the SFL process - the first such demonstration in a non-PDMS channel. We successfully synthesize homogeneous, multifunctional anisotropic particles in PFPE devices using SFL. PFPE-based SFL can cause the reduction of synthesis throughput due to low elastic modulus of PFPE channels. Apart from this disadvantage, PFPE-based SFL can exhibit more performances than the PDMS-based SFL. We quantified the dimensions of particles synthesized in both processes and found negligible differences (sub-micron). Also, we used PFPE-based SFL to synthesize multifunctional particles, showing that the technique can be compatible with the particle synthesis process on the structured microflows. Of particular interest, we demonstrate that PFPE-based SFL allows for the synthesis of anisotropic particles from precursors dissolved in organic solvents, a technique not possible with PDMS-based SFL. As one demonstrative application, we synthesize anisotropic particles from nonpolar organic precursors with stable dispersion of upconverting nanocrystals (UCNs).

Results and Discussion

Oxygen Inhibited Radical Polymerization on PFPE Surfaces

Before fabricating PFPE microfluidic channels and exploring SFL process in the channels, we designed a simple experiment to check whether the PFPE-silicone elastomer could provide oxygen lubrication layers for SFL (Fig. 1). In this experiment, we prepared precursor solutions that consisted of polyethylene glycol diacrylate (PEGDA) 700 and photoinitiator (PI) and sandwiched a droplet of the precursor solutions between substrates. The droplet then spread, forming a thin precursor layer. After droplet spreading, we used a 75 ms UV exposure to generate mask-defined polymerized structures in the sandwiched precursor layer. Typically, photocrosslinked PEGDA structures between glass slides adhered to the glass surfaces. Due to the oxygen impermeability of glass, the radical polymerization between glass slides was able to propagate to the glass surfaces without inhibition and thereby generated photo-patterned structures that were affixed to the surfaces (Fig. 1a). However, the photo-polymerized PEGDA structures between the PFPE layers were mobile immediately after UV exposure (Fig. 1b). In this case, the PEG structures were moved following the precursor liquid that flowed towards outside of the open system. This result demonstrated that the oxygen permeability of PFPE elastomer is sufficient to create oxygen lubrication layers that inhibit radical polymerization near surfaces and hence generation of free particles in solution.

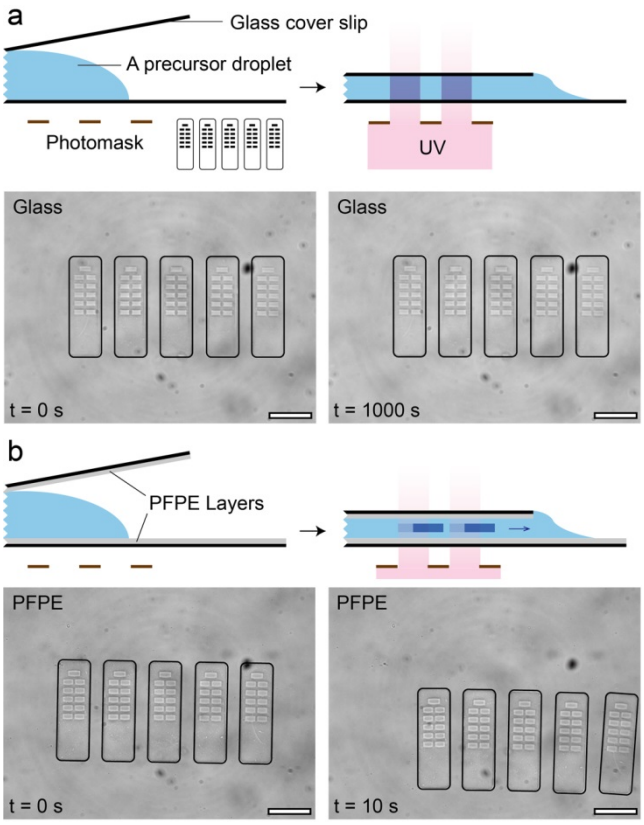

Fig.1 Oxygen permeable perfluoropolyether (PFPE) (a) A schematic depicting a control experiment to check the absence of oxygen lubrication layers on glass slides. When a droplet of PEGDA/PI is sandwiched between glass slides, the precursor liquid is flowed towards outside of the open system. Then, mask-defined shapes are printed on the precursor liquid by a 75 ms burst of UV light. The photopolymerized PEGDA structures (outlined for clarity) between glass slides were immobile even after 1000 seconds. (b) The same experiment was performed on glass slides that are coated with PFPE layers. Photo-polymerized PEGDA structures (outlined for clarity) between the PFPE layers were mobile just after UV exposure. This validated that PFPE could provide oxygen lubrication layers. Scale bars are 100 µm.

PFPE-based Stop Flow Lithography

With a motivation based on the preliminary result, we prepared PFPE devices via the literature procedures. Then, we used SFL to generate microparticles inside the devices. As expected, we found oxygen lubrication layers allowed for the fabrication of mobile particulates, and we successfully synthesized triangular particles that could be advected with the flow following synthesis (Fig. 2a and b). In the experiment, we used PEGDA 700 monomer to provide a benchmark against which PFPE devices can be compatible with a broad range of water-based precursor materials without swelling during the SFL operation. In the particle synthesis step, we stopped the monomer flow via pressure release for 300 ms, polymerized an array of the particles by a 75 ms exposure of UV light, and re-initiated the pressure-driven flow for 500 ms to flush particles out to the reservoir. This process was

Published on 07 October 2014. Downloaded on 07/10/2014 16:17:00.

Lab on a Chip Accepted Manuscript

View Article Online
DOI: 10.1039/C4LC00877D

repeated for several hours, showing that PFPE devices can be used for the SFL process for the mass-production of particles. We also explored the capabilities of PFPE devices in the production of multifunctional particles on structured microflows (Fig. 2c). We prepared PFPE devices with three inlets and generated three phase laminar flows inside the devices. We then controlled the relative widths of the streams by adjusting the inlet pressures, and we synthesized multifunctional barcoded particles on parallel flows with different widths. As seen in the fluorescent image of Figure 2c, the three regions in the barcoded particles were clearly separated from each other with sharp interfaces. Also, the holes in code regions had the same dimensions with mask design. The mask dimensions of numbers "1", "2", and "3" were 12×15 μm, 12×27.5 μm, and 12×40 μm, respectively. These results demonstrated that the typical SFL control over sharpness of interfaces of striped particles and edges of particle shapes can be achieved in PFPE devices.

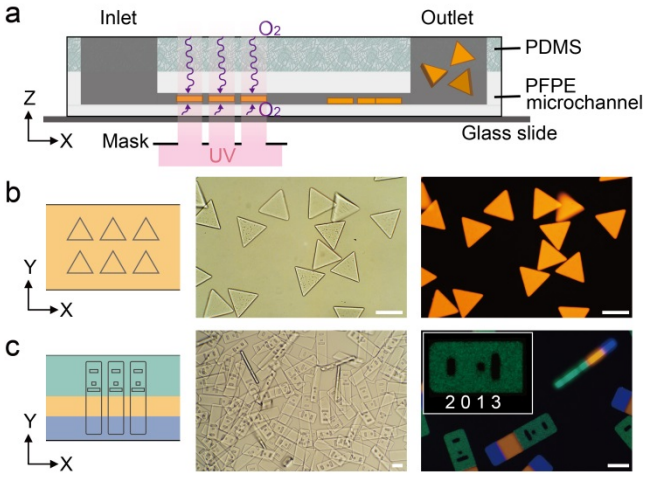

Fig. 2 Stop Flow Lithography (SFL) in a PFPE device (a) A schematic depicting the synthesis of triangular particles by SFL in a PFPE device. By virtue of oxygen lubrication layers, PFPE devices can allow for the production of free-floating particles. (b) The inserted schematic shows a top view of the process (a). Bright-field and fluorescent images show particles synthesized in (a). (c) Synthesis of multifunctional barcoded particles. A mask with an array of barcode particle shapes was aligned on three phase laminar flows that were created in a PFPE device with multiple inlets. Bright-field and fluorescent images show the barcoded particles with three distinct compartments. The inserted image shows a code region of the barcoded particles with code "2013". Scale bars are 100 μm (b) and 70 μm (c).

Comparison with PDMS-based Flow Lithography

The elastic modulus of the PFPE channels is around four times lower than the modulus of PDMS channels (Table 1), requiring longer channel relaxation time:

$$\frac{\tau_{r,PFPE}}{\tau_{r,PDMS}} \sim \frac{E_{PDMS}}{E_{PFPE}} = \frac{1.0\ \ MPa}{0.25\ \ MPa}$$

where $\tau_{r,PFPE}$ is the response time in PFPE devices, $\tau_{r,PDMS}$ is the response time in PDMS devices, E_{PDMS} is the Young's modulus of PDMS, and E_{PFPE} is the Young's modulus of PFPE. The requirement can cause the increase of the lag times associated with pulsed flow, and the decrease of particle synthesis throughput. Considering the SFL process time scales at the maximum throughput[2], we estimated the reduction rates of particle throughput in PFPE devices. The elastic PFPE channels caused around 25% reduction of the maximum SFL throughput.

Table 1 Summary of properties of PDMS and PFPE for SFL process

Properties	PDMS	PFPE	Source
elastic modulus	1.0 (MPa)	0.25 (MPa)	measured
oxygen permeability	550 (barrers)	400 (barrers)	ref 41

Like PDMS, PFPE is optically transparent and compatible with standard flow lithography techniques. The optical properties of our device are further described in Supplementary Information. Also, as the oxygen permeability of PFPE is close to the value of PDMS, PFPE can provide similar oxygen lubrication layers to PDMS (Table 1). To demonstrate that PFPE devices can exhibit the SFL performance analogous to PDMS devices, we produced particles in both devices under the same SFL conditions and compared the dimensions of produced particles. As we used 15 μm circular masks and 25 μm high channels, we generated cylindrical particles with aspect ratios greater than 1. The aspect ratio of particles was defined to be the ratio of the overall particle height divided by the size of the feature produced by the transparency mask. We estimated particle widths from differential interference contrast images that were instantly captured after particle polymerization (Fig. 3a). Also, as particles with the aspect ratios greater than 1 were toppled by flow, we easily measured the heights of particles produced from each device (Fig. 3b). In PDMS devices, the width of particles was 14.4 μm while the height of particles was 21.8 μm (Fig. 3a). In PFPE devices, the width of particles was 13.5 μm while the height of particles was 21.2 μm (Fig. 3b). The coefficient of variations in particle widths and heights were the same for both PDMS and PFPE devices as 0.01 and 0.03. The small values implied the particle synthesis was performed in a highly reproducible manner. Importantly, the differences in the dimensions of the particles fabricated in the different devices were below 1 μm. These results quantitatively demonstrate that PFPE-based SFL can provide the particle synthesis control akin to PDMS-based SFL.

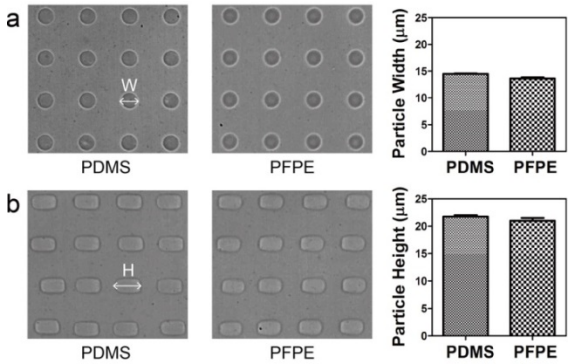

Fig.3 Comparison of SFL performance between PDMS and PFPE devices (a) Top view of particles synthesized in both devices. The cylindrical particles were synthesized by SFL process using a mask with an array of 15 μm circles. For both devices, the widths (W) of sixteen particles were measured and plotted. The error bars indicate standard deviation. (b) Side view of particles. The particles were toppled by stable laminar flow in microfluidic devices. Like (a), the particle heights (H) were measured and plotted with error bars.

Published on 07 October 2014. Downloaded on 07/10/2014 16:17:00.

Lab on a Chip Accepted Manuscript

View Article Online
DOI: 10.1039/C4LC00877D

Published on 07 October 2014. Downloaded on 07/10/2014 16:17:00.

Lab on a Chip Accepted Manuscript

Organic Solvent Resistance in PFPE-based Flow Lithography

The most valuable feature of PFPE devices is that the devices are compatible with most organic solvents. In both PDMS and PFPE devices, we synthesized 250 μm long bar-shaped particles from polyurethane (PU) monomers dissolved in toluene (Fig. 4a and d). We used toluene because it is an organic solvent that is known to severely swell PDMS[24]. The particle shape was chosen to investigate channel shape after swelling on the coordinate of channel width. Also, the PU monomer was selected as an exemplary hydrophobic monomer among a wide range of water-insoluble monomers. This UV curable hydrophobic monomer has been used for the preparation of replica molds that have patterns with sub-100nm feature resolutions and low surface energy comparable to PDMS[45]. In addition, PU has provided biocompatibility for the construction of scaffolds in tissue engineering[46, 47]. Recently, Janus PU microfiber scaffolds that contained porous and non-porous compartments have shown great improvement of cell adhesion, proliferation, and viability[48]. Anisotropic PU particles could offer distinct advantages over immobile PU molds or scaffolds as particle templates and building blocks to construct complex and dynamic tissues.

We can easily modulate the PU composition in toluene to tune both chemical and mechanical properties of the microparticles. During the PU particle synthesis, we mixed the PU precursors with a toluene solution at a 1:1 volume ratio. In the experiments, the particles synthesized in PDMS devices were deformed, reflecting a swollen channel (Fig. 4b). The particles synthesized in PFPE devices, by comparison, were flat without shape distortion (Fig. 4e). We further quantified the fluorescent signals on the particle distance (Fig. 4c and f). The fluorescent signal of particles synthesized in PDMS devices was two times lower than the signal of particles synthesized in PFPE devices, validating that the former particles were thinner than the latter. Also, the particles synthesized in the PDMS device emitted concave fluorescent signals, indicative of deformed particles. This result clearly demonstrated that PFPE devices can be used to synthesize anisotropic particles using organic solvents.

Recently, we developed oxygen-free FL that enables SFL process in wide ranges of solvent resistant devices[49]. However, the device fabrication process in oxygen-free FL is somewhat complex as the devices should be prepared as 3D channels for flow-stacking. PFPE devices can be an efficient platform for SFL with organic solvents without flow stacking process.

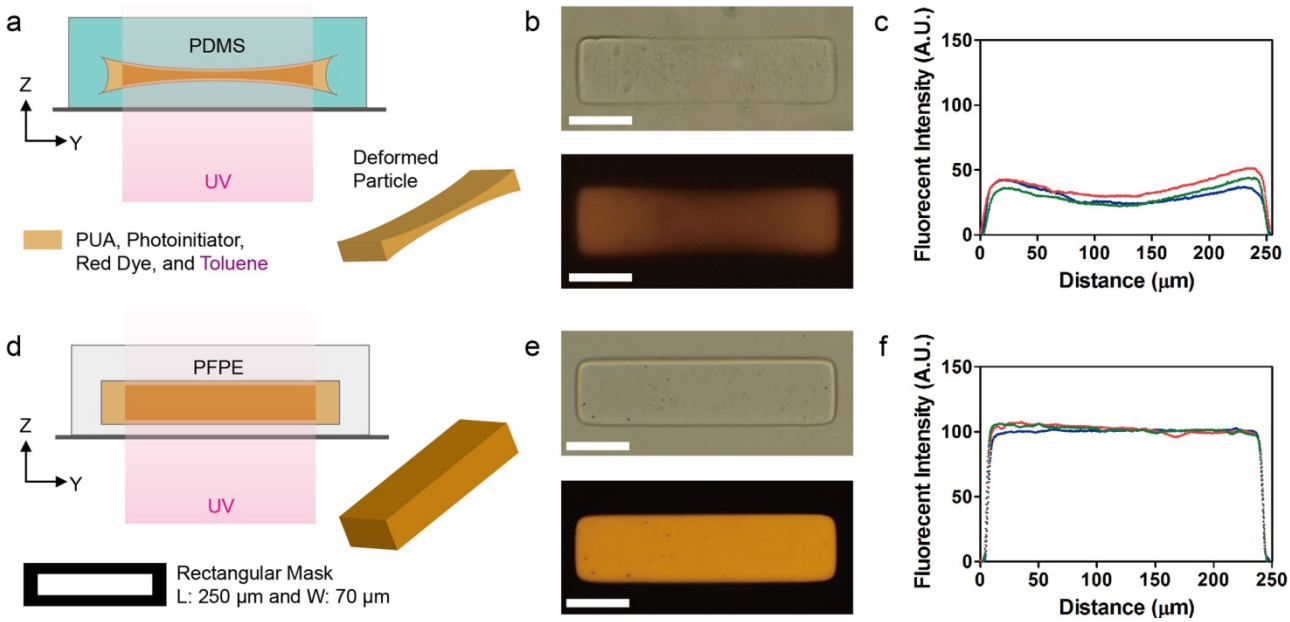

Fig.4 Comparison of organic solvent-based SFL between PDMS and PFPE devices (a) A schematic depicting toluene-based SFL process in PDMS devices. The particles have curved shapes due to the swelling of the PDMS walls. The precursor consists of water insoluble monomer (polyurethane acrylate (PUA)), toluene, photoinitiator, and rhodamine acrylate. (b) Bright-field and fluorescent miscopy images of curved particles. (c) The fluorescent signals of three particles were quantitatively analyzed on particle distance using Image J software. (d) A schematic depicting toluene-based SFL process in PFPE devices. The particles have flat shapes due to toluene resistance of PFPE devices. (e) Bright-field and fluorescent images of flat particles. (f) Like (c), the fluorescent signals of three particles were analyzed on particle distance. Scale bars are 70 μm.

View Article Online
DOI: 10.1039/C4LC00877D

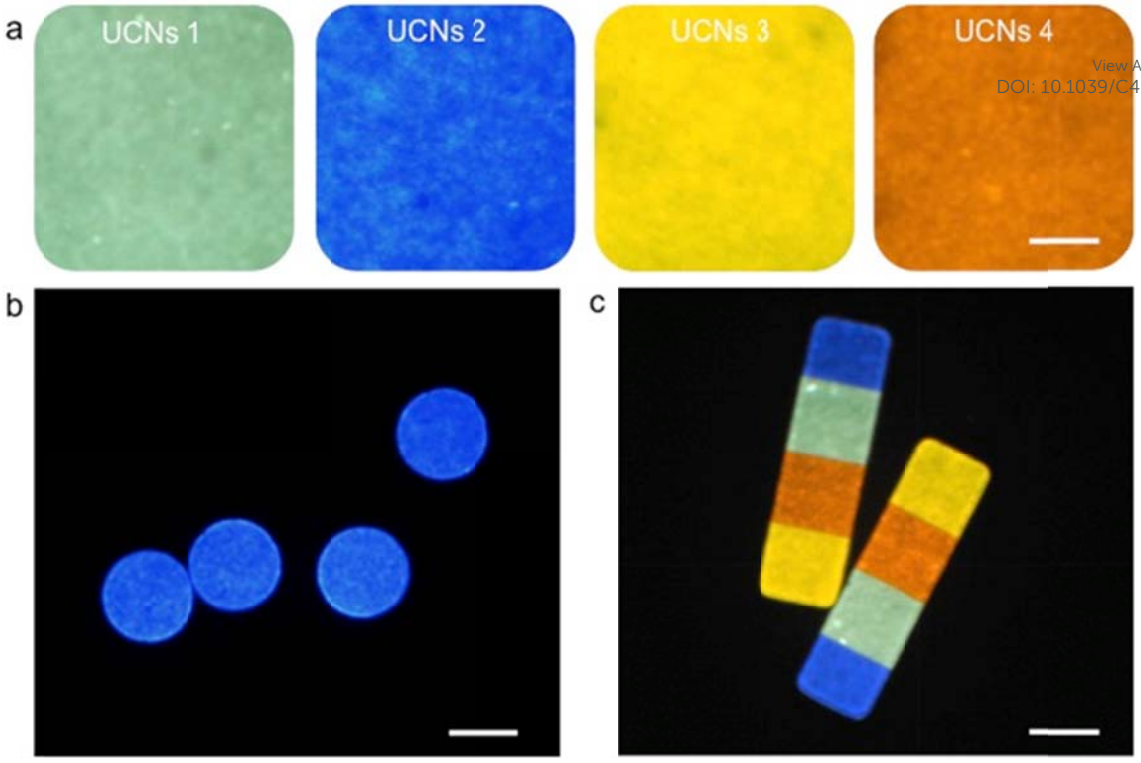

Fig. 5. (a) Luminescence image of UCNs 1-4 in PUA monomer solution (PUA, cyclohexane, photoinitiator) (left to right), (b) Luminescence image of UCNs embedded microparticles, and (c) Homogeneous luminescence image of UCNs embedded striped microparticles (980 nm excitation). Scale bars are 50 μm.

Synthesis of UCNs-laden microparticles

To extend the applicability of PFPE-based SFL, we synthesized UCNs-laden microparticles in a PFPE device. We have recently demonstrated UCNs embedded microparticle synthesis for the anti-counterfeiting application.[50] In this work, mono-dispersed hexagonal phase UCNs were stabilized with oleic acid during the hydrothermal synthesis and successfully incorporated in PU microparticles using PDMS device. It is known that the fluorescence emission of hydrophobic UCNs is quenched in polar solvents such as ethanol and water due to aggregation. Therefore, UCNs were dispersed in a nonpolar organic solvent (cyclohexane) after the synthesis. However, cyclohexane is known to swell PDMS and therefore incompatible with standard PDMS-based SFL.[24] To process the UCNs in SFL we had to completely remove cyclohexane from the UCNs solution and re-dispersed them in photocurable monomer solution through strong sonication. This process is tedious, time consuming and requires careful attention to avoid possible undesired polymerization of monomer by heat. Furthermore, the removal of all the solvent takes away a useful handle to modulate porosity of the synthesized PU particles for further applications.

To overcome these challenges, we employed a PFPE device to synthesize the UCNs-laden microparticles using a photocurable resin containing a nonpolar organic solvent. We prepared homogeneously dispersed UCNs solution in PU monomer composed of 50% [v/v] PU, 40% UCNs in cyclohexane (0.1mg/ul), 10% [v/v] Darocur 1173 (Fig. 5a). As can be seen in Fig 5b, UCNs laden-microparticles synthesized in PFPE device emitted homogeneous visible spectrum. We also successfully synthesized striped microparticles with PU monomers containing a nonpolar organic solvent and without losing their homogeneous emission property. This demonstrative example shows the future utility of the PFPE devices for particle synthesis when using nonpolar organic solvents.

Experimental

Materials

The liquid PFPEs kit (SIFEL X71-8115) was kindly provided by Shin-Etsu Co. This product has two parts: (1) Part A that consists of a PFPE backbone capped with vinyl silicone and (2) Part B that consists of a PFPE backbone capped with silicon hydride. Also, PUA blend (MINS 311RM) was kindly provided by Minuta tech. PDMS (Sylgard 184) kit was purchased from Dow Corning Co. PEGDA 700, PEG200, and Darocur1173 photoinitiator (2-hydroxy-2-methylpropiophenon) were purchased from Sigma Aldrich, and used as received. In Figure 1, the composition of the PEG precursor solutions was of 5% (v/v) Darocur 1173, 40% (v/v) 3X Tris-EDTA (TE) buffer, 25% (v/v) PEG 200, and 30% (v/v) PEGDA. In Figure 2a, the triangular particles were made using solutions of 5% (v/v) Darocur 1173, 39% (v/v) 1X Tris-EDTA (TE) buffer, 20% (v/v) PEG 200, 35% (v/v) PEGDA, and 1% (v/v) methacryloxyethyl thiocarbamoyl rhodamine B (Polysciences) in PEG 200 (1mg/ml). In Figure 2b, the top stream consists of 5% (v/v) Darocur 1173, 35% (v/v) 1X Tris-EDTA (TE) buffer, 20% (v/v) PEG 200, 35% (v/v) PEGDA, and 5% (v/v) 200 nm green fluorescent (Fluoresbrite Yellow-Green

Published on 07 October 2014. Downloaded on 07/10/2014 16:17:00.

Lab on a Chip Accepted Manuscript

View Article Online
DOI: 10.1039/C4LC00877D

Carboxylate Microspheres, Polysciences). The middle stream had the same composition with the solution in Figure 2a. The bottom stream was the same composition as the previous top stream, except 5% (v/v) of the green fluorescent beads was replaced with 100 nm blue fluorescent beads (Fluoresbrite Blue Carboxylate Microspheres, Polysciences). All of the particles in Figure 3 were made using solutions of 5% (v/v) Darocur 1173, 94% (v/v) PEGDA, and 1% (v/v) methacryloxyethyl thiocarbamoyl rhodamine B (Polysciences) in PEG 200 (1mg/ml). All of the particles in Figure 4 were made from 4% (v/v) Darocur 1173, 45% (v/v) PUA, 50% (v/v) Toluene, and 1% (v/v) methacryloxyethyl thiocarbamoyl rhodamine B (Polysciences) in PEG 200 (1mg/ml). Finally, composition of the photocurable monomer solution in Figure 5 is 50% (v/v) PUA, 40% (v/v) UCNs in cyclohexane (0.1mg/ul), and 10% (v/v) Darocur 1173.

Device Fabrication

PFPE devices are prepared via the previous literature procedures[44, 51]. Briefly, glass slides were coated with B-rich SIFEL (mixed at 1:1.5 Part A: Part B) and partially cured at 110 ˚C for 30 min. The coating thickness was around 200 µm which was thick enough to transport oxygen into the device. Then, A-rich SIFEL (mixed at 1.5:1) was coated over an SU-8 master (Stanford Foundry), and cured at 110 ˚C for 10 min. After that, PDMS (mixed at 10:1 base:curing agent) was poured on the SIFEL layer to add device thickness and save SIFEL material. In particular, the addition of PDMS to the SIFEL layer can offer the enhanced mechanical strength to the devices, prevent the wrinkling problems during the heat curing, and reduce the fabrication costs[44, 51]. The composite layer was further cured at 80 ˚C for 45 min. Lastly, the A-rich SIFEL channel was combined with the B-rich SIFEL coated glass at 120 ˚C for 45 min. PDMS channels are generated by pouring PDMS over an SU-8 master, and then curing 2 hrs at 60 ˚C in an oven. Then, glass slides were coated with PDMS and partially cured at 60 ˚C for 25 min. To finish the construction of PDMS devices, PDMS channels were assembled on the PDMS-coated glass slides, and the devices were fully cured at 60 ˚C for 2 hrs.

Photopolymerization Setup

Devices were mounted on an inverted microscope (Axiovert 200, Zeiss) equipped with a VS25 shutter system (UniBlitz) to precisely control the UV exposure dose. A photomask was then inserted into the field-stop of the microscope. The masks were designed in AUTOCAD 2010 and printed using a high-resolution printer at CAD Art Services (Bandon, OR). A Lumen 200 (Prior) served as the source of UV light. A filter set that allowed wide UV excitation (11000v2: UV, Chroma) was used to select light of the desired wavelength. The VS25 shutter system driven by a computer-controlled VMM-D1 shutter driver provided specified pulses of UV light. The shutter-mediated UV exposures were synchronized with the stop flow system using Python to allow the user to cycle SFL process automatically through the specification of a flow duration, a stoppage duration, and an exposure time. We used 500 ms flow time, 300 ms stop time, and 75 ms exposure time during the particle synthesis.

Stop Flow Lithography Setup

Rapid alternation between the flow and stoppage states was achieved with the compressed-air flow control system. The setups of the pressure-driven flow system are precisely described in our previous work[52]. Briefly, a compressed air source (~40 psi) was connected to a high-pressure regulator (150 psi maximum outlet, Dayton), which in turn was connected to a low-pressure regulator (0.5 – 25 psi outlet range, ControlAir, Inc.) equipped with a digital gauge (Type 100 LR, Omega). Downstream of the regulators, a three-way solenoid valve (Model 6014, Burkert) was used to switch rapidly between atmospheric pressure (stop) and the input pressure (flow). The output from the three-way valve was connected to the microfluidic device using Tygon tubing connected to a 200 µl pipette tip (Biosciences). The pipette tip was filled with the desired fluid and inserted into the inlet hole punched in the microfluidic device. On this setup, the rapid pulsing of microflows was generated within the microfluidic device using the script-controlled solenoid valve.

Particle Recovery

PEG particles synthesized using SFL are collected in a 650 µl Eppendorf tube, and suspended in 1× Tris-EDTA with 0.05% Tween-20 (Sigma Aldrich). We removed unreacted monomer and fluorescent dyes from the suspension by rinsing with 1× Tris-EDTA with 0.05% Tween-20, centrifuging the particle sample, and removing excess rinsing solution. After repeating the rinsing procedures 10 times, the cleaned particles were stored in 300 µL of solution in an Eppendorf tube for imaging. PU particles were also washed with the same procedures except the rinsing solution was replaced as ethanol with 0.05% Tween-20 to dissolve unreacted hydrophobic PUA monomers.

Imaging for Quantitative Analysis

For the microparticles inside microfluidic devices, images were directly captured from a complementary metal oxide semiconductor (CMOS) camera (DMK 41BUC02, Imaging Source) mounted to the side port of the inverted microscope (Axiovert 200, Zeiss). The camera was controlled by IC capture software. For the microparticles suspended in a collection tube, we fabricated reservoirs by sealing a PDMS rectangular frame (5 × 5 × 5 mm) onto a PDMS-coated glass slide. Each reservoir was filled with the particles suspended in 1× Tris-EDTA with 0.05% Tween-20 or ethanol with 0.05% Tween-20. The reservoirs were then mounted on the microscope, and the images of microparticles were captured using IC capture software or a digital camera (D200, Nikon) and Nikon Capture software. Images were further analyzed using Image J.

Measuring Elastic Modulus

The elastic modulus of PDMS and PFPE was measured using a stress-controlled rheometer (ARG-2, TA Instruments, New Castle, DE) with a 20 mm diameter aluminium plate geometry and with the temperature controlled to 25 ºC. After cylindrical elastomer samples with 20 mm diameter were placed in the rheometer, the elastic and shear modulus were measured through frequency sweep from 0 to 100 rad/s. The elastic modulus that we reported was averaged values over the frequencies. As the elastic modulus kept constant in experiments with three different kinds of strains (0.01%, 0.05%, and 0.1%), the linear regime of strain-stress was confirmed.

Published on 07 October 2014. Downloaded on 07/10/2014 16:17:00.

Lab on a Chip Accepted Manuscript

View Article Online
DOI: 10.1039/C4LC00871D

Published on 07 October 2014. Downloaded on 07/10/2014 16:17:00.

Lab on a Chip Accepted Manuscript

Synthesis of UCNs

UCNs were synthesized as described previously.[53] 3.0 mL of NaOH (0.6 g) solution was mixed with 10 mL of ethanol and 10 mL of oleic acid under vigorous stirring. 2 mL of $RECl_3$ (0.2 M, RE = Y, Yb, Er, Gd) and 2 mL of NH_4F (2 M) were then added dropwise into the mixture. The solution was transferred to a 50 mL Teflon-lined autoclave and heated at 200 ºC for 2 h. The autoclave was allowed to cool naturally to room temperature. Ethanol was used to collect the precipitated products, which were then purified by centrifugation, washed several times with ethanol and DI water, and finally re-dispersed in cyclohexane.

Table 2 Composition of synthesized UCNs (mol %)

	UCNs1	UCNs2	UCNs3	UCNs4
Gd	30	30	30	30
Y	49.7	51.8	38	-
Yb	20	18	30	68
Er	0.1	-	2	2
Tm	0.2	0.2	-	-

Conclusions

We have demonstrated that PFPEs are an alternative material for microfluidic devices used in SFL. PFPEs are commercially available, compatible with soft lithography, optically transparent, and permeable to oxygen. We showed that similar SFL performance can be achieved in both PFPE and PDMS devices - the particles produced from both devices showed negligible differences in shapes and sharpness of interfaces of striped particles. As PFPE has a lower elastic modulus than PDMS, the PFPE channels can extend lag times in the SFL process and decrease the particle throughput. However, we highlight the PFPE devices are compatible with most organic solvents, allowing for the solvent-based SFL that can achieve particles with higher degree of chemical complexity than the prior PDMS-based SFL. We believe that the PFPE-based SFL can be a simple but powerful technique to create new class of multifunctional particles from organic precursors.

Acknowledgements

We gratefully acknowledge the support of Kwanjeong Educational Foundation, the Singapore-MIT Alliance, the National Science Foundation grant CMMI-1120724 and DMR-1006147. We also thank Dr. Nakwon Choi for useful discussions, Ben Renner for comments on the manuscript, and Dr. H. Burak Eral for his assistance in measuring elastic modulus.

References

1. D. Dendukuri, D. C. Pregibon, J. Collins, T. A. Hatton and P. S. Doyle, *Nat Mater*, 2006, **5**, 365-369.
2. D. Dendukuri, S. S. Gu, D. C. Pregibon, T. A. Hatton and P. S. Doyle, *Lab Chip*, 2007, **7**, 818-828.
3. J. H. Jang, D. Dendukuri, T. A. Hatton, E. L. Thomas and P. S. Doyle, *Angew Chem Int Ed*, 2007, **46**, 9027-9031.
4. K. W. Bong, D. C. Pregibon and P. S. Doyle, *Lab Chip*, 2009, **9**, 863-866.
5. K. W. Bong, K. T. Bong, D. C. Pregibon and P. S. Doyle, *Angew Chem Int Ed*, 2010, **49**, 87-90.
6. S. C. Laza, M. Polo, A. A. R. Neves, R. Cingolani, A. Camposeo and D. Pisignano, *Adv Mater*, 2012, **24**, 1304-1308.
7. D. C. Pregibon, M. Toner and P. S. Doyle, *Science*, 2007, **315**, 1393-1396.
8. S. C. Chapin, D. C. Appleyard, D. C. Pregibon and P. S. Doyle, *Angew Chem Int Ed*, 2011, **50**, 2289-2293.
9. H. Lee, J. Kim, H. Kim, J. Kim and S. Kwon, *Nat Mater*, 2010, **9**, 745-749.
10. K. W. Bong, S. C. Chapin and P. S. Doyle, *Langmuir*, 2010, **26**, 8008-8014.
11. D. C. Appleyard, S. C. Chapin, R. L. Srinivas and P. S. Doyle, *Nature Protocols*, 2011, **6**, 1761-1774.
12. S. E. Chung, W. Park, S. Shin, S. A. Lee and S. Kwon, *Nat Mater*, 2008, **7**, 581-587.
13. D. Dendukuri, T. A. Hatton and P. S. Doyle, *Langmuir*, 2007, **23**, 4669-4674.
14. P. Panda, K. W. Bong, T. A. Hatton and P. S. Doyle, *Langmuir*, 2011, **27**, 13428-13435.
15. R. F. Shepherd, P. Panda, Z. Bao, K. H. Sandhage, T. A. Hatton, J. A. Lewis and P. S. Doyle, *Adv Mater*, 2008, **20**, 4734-4739.
16. H. Kim, J. Ge, J. Kim, S. Choi, H. Lee, H. Lee, W. Park, Y. Yin and S. Kwon, *Nat Photonics*, 2009, **3**, 534-540.
17. P. Panda, S. Ali, E. Lo, B. G. Chung, T. A. Hatton, A. Khademhosseini and P. S. Doyle, *Lab Chip*, 2008, **8**, 1056-1061.
18. D. C. Duffy, J. C. McDonald, O. J. A. Schueller and G. M. Whitesides, *Anal Chem*, 1998, **70**, 4974-4984.
19. M. Li, M. Humayun, J. A. Kozinski and D. K. Hwang, *Langmuir*, 2014, DOI: 10.1021/la501723n.
20. J. C. McDonald, D. C. Duffy, J. R. Anderson, D. T. Chiu, H. K. Wu, O. J. A. Schueller and G. M. Whitesides, *Electrophoresis*, 2000, **21**, 27-40.
21. T. J. Johnson, D. Ross, M. Gaitan and L. E. Locascio, *Anal Chem*, 2001, **73**, 3656-3661.
22. S. K. Sia and G. M. Whitesides, *Electrophoresis*, 2003, **24**, 3563-3576.
23. D. Dendukuri, P. Panda, R. Haghgooie, J. M. Kim, T. A. Hatton and P. S. Doyle, *Macromolecules*, 2008, **41**, 8547-8556.
24. J. N. Lee, C. Park and G. M. Whitesides, *Anal Chem*, 2003, **75**, 6544-6554.
25. D. Bartolo, G. Degre, P. Nghe and V. Studer, *Lab Chip*, 2008, **8**, 274-279.
26. C. F. Carlborg, T. Haraldsson, K. Oberg, M. Malkoch and W. van der Wijngaart, *Lab Chip*, 2011, **11**, 3136-3147.
27. E. Sollier, C. Murray, P. Maoddi and D. Di Carlo, *Lab Chip*, 2011, **11**, 3752-3765.
28. L. H. Hung, R. Lin and A. P. Lee, *Lab Chip*, 2008, **8**, 983-987.
29. D. Ogonczyk, J. Wegrzyn, P. Jankowski, B. Dabrowski and P. Garstecki, *Lab Chip*, 2010, **10**, 1324-1327.
30. J. F. Chen, M. Wabuyele, H. W. Chen, D. Patterson, M. Hupert, H. Shadpour, D. Nikitopoulos and S. A. Soper, *Anal Chem*, 2005, **77**, 658-666.
31. P. Kim, H. E. Jeong, A. Khademhosseini and K. Y. Suh, *Lab Chip*, 2006, **6**, 1432-1437.

View Article Online
DOI: 10.1039/C4LC00877D

32. R. Barrett, M. Faucon, J. Lopez, G. Cristobal, F. Destremaut, A. Dodge, P. Guillot, P. Laval, C. Masselon and J. B. Salmon, *Lab Chip*, 2006, **6**, 494-499.
33. K. I. Min, T. H. Lee, C. P. Park, Z. Y. Wu, H. H. Girault, I. Ryu, T. Fukuyama, Y. Mukai and D. P. Kim, *Angew Chem Int Ed*, 2010, **49**, 7063-7067.
34. M. C. Park, J. Y. Hur, K. W. Kwon, S. H. Park and K. Y. Suh, *Lab Chip*, 2006, **6**, 988-994.
35. H. E. Jeong and K. Y. Suh, *Lab Chip*, 2008, **8**, 1787-1792.
36. L. Brown, T. Koerner, J. H. Horton and R. D. Oleschuk, *Lab Chip*, 2006, **6**, 66-73.
37. K. N. Ren, W. Dai, J. H. Zhou, J. Su and H. K. Wu, *P Natl Acad Sci USA*, 2011, **108**, 8162-8166.
38. A. Asthana, Y. Asthana, I. K. Sung and D. P. Kim, *Lab Chip*, 2006, **6**, 1200-1204.
39. A. R. Abate, D. Lee, T. Do, C. Holtze and D. A. Weitz, *Lab Chip*, 2008, **8**, 516-518.
40. B. Y. Kim, L. Y. Hong, Y. M. Chung, D. P. Kim and C. S. Lee, *Adv Funct Mater*, 2009, **19**, 3796-3803.
41. J. P. Rolland, R. M. Van Dam, D. A. Schorzman, S. R. Quake and J. M. DeSimone, *J Am Chem Soc*, 2004, **126**, 2322-2323.
42. Y. Y. Huang, P. Castrataro, C. C. Lee and S. R. Quake, *Lab Chip*, 2007, **7**, 24-26.
43. G. Maltezos, E. Garcia, G. Hanrahan, F. A. Gomez, S. Vyawhare, R. M. van Dam, Y. Chen and A. Scherer, *Lab Chip*, 2007, **7**, 1209-1211.
44. N. S. G. K. Devaraju and M. A. Unger, *Lab Chip*, 2011, **11**, 1962-1967.
45. S. J. Choi, P. J. Yoo, S. J. Baek, T. W. Kim and H. H. Lee, *J Am Chem Soc*, 2004, **126**, 7744-7745.
46. T. J. Dennes and J. Schwartz, *Soft Matter*, 2008, **4**, 86-89.
47. A. B. Jozwiak, C. M. Kielty and R. A. Black, *J Mater Chem*, 2008, **18**, 2240-2248.
48. J. H. Jung, C. H. Choi, S. Chung, Y. M. Chung and C. S. Lee, *Lab Chip*, 2009, **9**, 2596-2602.
49. K. W. Bong, J. J. Xu, J. H. Kim, S. C. Chapin, M. S. Strano, K. K. Gleason and P. S. Doyle, *Nat Commun*, 2012, **3**, 805.
50. J. Lee, P. W. Bisso, R. L. Srinivas, J. J. Kim, A. J. Swiston and P. S. Doyle, *Nat Mater*, 2014, **13**, 524-529.
51. T. J. A. Renckens, D. Janeliunas, H. van Vliet, J. H. van Esch, G. Mul and M. T. Kreutzer, *Lab Chip*, 2011, **11**, 2035-2038.
52. K. W. Bong, S. C. Chapin, D. C. Pregibon, D. Baah, T. M. Floyd-Smith and P. S. Doyle, *Lab Chip*, 2011, **11**, 743-747.
53. F. Wang, Y. Han, C. S. Lim, Y. Lu, J. Wang, J. Xu, H. Chen, C. Zhang, M. Hong and X. Liu, *Nature*, 2010, **463**, 1061-1065.

Published on 07 October 2014. Downloaded on 07/10/2014 16:17:00.

Lab on a Chip Accepted Manuscript